Iraqi National Journal of Earth Science
www.earth.mosuljournals.com

Major, Trace, and Rare Earth Elements Geochemistry of the Upper Miocene Injana Formation Sandstone, Northern Iraq: Provenance, Paleoclimate and Palaeoweathering

Anwaar S. Al-Maadhidi [1], **Mohamed W. Alkhafaji** [2*], **Lefta S. Kadhim** [3]

[1] *Department of Geology, College of Science, University of Kirkuk, Kirkuk, Iraq.*
[2,3] *Applied Geology Department, College of Science, University of Tikrit, Tikrit, Iraq.*

Article information

Received: 20- Nov -2023

Revised: 28- Feb -2024

Accepted: 25- Apr -2024

Available online: 01- Apr – 2025

Keywords:
Injana Formation
Provenance
Paleoclimate
Plaeoweathering
REE

Correspondence:
Name: Mohamed W. Alkhafaji

Email:
mohamed_wagga@yahoo.com

ABSTRACT

To determine the provenance, paleoclimate and palaeoweathering of the Upper Miocene sandstones of the Injana Formation, 12 sandstone samples from two sites (Mirawa and Degala) in Erbil Governorate, northern Iraq are investigated. Major, trace, and rare earth elements are measured using X-ray fluorescence (XRF) and inductively coupled plasma-mass spectrometry (ICP-MS). The elemental concentrations and ratios of the studied sandstones indicate their sources from intermediate to mafic igneous rocks. All the chondrite-normalized REEs samples are similar and exhibit a minor enrichment of light rare-earth elements (LREE) in comparison to the heavy rare earth elements (HREE) with a negligible negative europium (Eu) anomaly. The low to moderate values of the plagioclase index of alteration (PIA), chemical index of alteration (CIA), high values of index of compositional variability (ICV > 1), and the A-CN-K plot, all indicate a low to moderate chemically weathered source area. Palaeoclimatic information can be provided using the plot of the SiO_2 versus (Al_2O_3+Na_2O + K_2O) indicating that the deposition of Injana sandstones has occurred under fluctuated climate between arid to semi-arid.

DOI: 10.33899/earth.2024.143982.1162, ©Authors, 2025, College of Science, University of Mosul.
This is an open access article under the CC BY 4.0 license (http://creativecommons.org/licenses/by/4.0/).

جيوكيميائية العناصر الرئيسة والاثرية والأرضية النادرة للحجر الرملي لتكوين انجانة (المايوسين الأعلى)، شمالي العراق: المصدرية، المناخ القديم والتجوية القديمة

أنوار سويد جاسم المعاضيدي [1] ، محمد وكاع الخفاجي [*2] ، لفتة سلمان كاظم [3]

[1] *قسم علوم الارض، كلية العلوم، جامعة كركوك، كركوك، العراق.*

[3,2] *قسم علوم الأرض التطبيقية، كلية العلوم، جامعة تكريت، تكريت، العراق.*

معلومات الارشفة

تاريخ الاستلام: 20– نوفمبر –2023

تاريخ المراجعة: 28– فبراير –2024

تاريخ القبول: 25– ابريل –2024

تاريخ النشر الالكتروني: 01– ابريل –2025

الكلمات المفتاحية:
تكوين انجانة
المصدر
المناخ القديم
التجوية القديمة
عناصر الأرضية النادرة

المراسلة:

الاسم: محمد وكاع الخفاجي

Email: mohamed_wagga@yahoo.com

الملخص

لمعرفة المصدرية، المناخ القديم والتجوية القديمة للحجر الرملي من المايوسين الأعلى لتكوين إنجانة، تم فحص 12 نموذجا من الحجر الرملي من موقعين (ميراوا وديكلة) في محافظة أربيل. تم تحليل الأكاسيد الرئيسة والعناصر الثانوية والعناصر الأرضية النادرة بواسطة XRF و ICP–MS. تشير التراكيز ونسب العناصر الأرضية النادرة في الحجر الرملي إلى ان مصدرها هو صخور نارية متوسطة– مافية . جميع تراكيز العناصر الأرضية النادرة التي تمت معايرتها بالكوندرايت كانت متشابهة وتظهر اغناءً طفيفاً للعناصر الأرضية النادرة الخفيفة مقارنةً بالعناصر الأرضية النادرة الثقيلة مع شذوذ سلبي ضئيل في الأيروبيوم. يمتلك مؤشر تحلل البلاجوكليس (PIA) ومؤشر التغير الكيميائي (CIA) قيماً منخفضة الى متوسطة، بينما كانت قيم مؤشر التباين الكيميائي اكبر من 1 (ICV > 1)، ويشير مخطط A– CN–K إلى أن التجوية الكيميائية كانت منخفضة الى متوسطة في منطقة الدراسة. يشير الرسم البياني لـ SiO_2 مقابل ($Al_2O_3+Na_2O$ + K_2O) إلى المناخ الجاف إلى شبه الجاف أثناء ترسب الحجر الرملي لتكوين إنجانة.

DOI: 10.33899/earth.2024.143982.1162, ©Authors, 2025, College of Science, University of Mosul.
This is an open-access article under the CC BY 4.0 license (http://creativecommons.org/licenses/by/4.0/).

Introduction

The provenance, degree of transportation, diagenesis processes, and depositional environment, all influence the composition of siliciclastic rocks (Garzanti *et al.*, 2008). The chemical composition is influenced by the type of their source rocks as well as chemical weathering and diagenesis (Nesbitt *et al.*, 1996). Sandstone mineralogy and petrography are being extensively utilized to define their origin (Garzanti, 2019), whereas the paleoclimate, provenance, tectonic setting, and paleoweathering of the sandstone are all determined using the bulk rock geochemistry of the material (Cullers, 2000). To recreate the source rock composition, provenance, paleoclimate, paleoweathering, and depositional tectonic context of siliciclastic rocks, the chemical composition, mineralogy, and petrography of these rocks are extensively used (McLennan and Taylor, 1991; Roddaz *et al.*, 2011; Zaid *et al.*, 2015; Löwen *et al.*, 2018; Ge *et al.*, 2019; Chen and Robertson, 2020; Moghaddam *et al.*, 2020). The utilization of trace elements for provenance interpretation is dependent on their relative stability. Because the high field strength elements (HFSE such as Th, Y, Nb, Zr) are generally immobile, therefore they can be used as indicators of provenance (Taylor and McLennan, 1985). Additionally, markers of provenance can be found in the ratios of incompatible to compatible elements (for instance, Th/Sc, La/Sc, Zr/Sc, and Th/Co) (McLennan *et al.*, 1983; Yan *et al.*, 2007). CIA (chemical index of alteration; Nesbitt and Young, 1982) and CIW (chemical index of weathering; Harnois, 1988) are widely used to infer the intensity of weathering of the sediments and rocks (Roy *et al.*, 2008).

The studied sandstone samples are collected from two different sites, Degala and Mirawa. In both areas, the formation has a thickness of 168 and 133 m respectively. At the two sites, the lower contact with the Fat'ha Formation is gradational and established by the first occurrence of the gypsum layer. The initial occurrence of the pebbly sandstone bed serves as a gradational indicator of the upper contact with the Mukdadiya Formation.

Injana Formation sandstones are fine to coarse-grained, of red to grey color, hard to friable, laminated to thickly bedded, and sometimes interbedded with thin layers of mudstone. Several types of sedimentary structures may be recognized like cross-bedding, lamination, ripple mark and bioturbation (Fig. 1).

The Upper Miocene Injana Formation is widely distributed in Iraq, and it is quite significant in terms of raw materials and economics (Al-Rawi *et al.*, 1992). It is made up of clastic sediment deposits in a fluviatile environment. It is intensively investigated due to its widespread distribution, but the majority of these investigations concentrated on mineralogy, sedimentology and the depositional environment (Al-Sammarai, 1978; Al-Juboury,1994; Mahdi, 2006; Jassim and Goff, 2006). Petrography and provenance studies of the Injana Formation sandstones were provided by Al-Salmani and Tamar-Agha (2018), who believe that the Injana Formation's provenances are mainly igneous and sedimentary rocks as well as metamorphic rocks. The sandstones of Injana Formation are mainly immature litharenite. Whereas Al-Juboury et al. (2009) investigated the geochemistry of the Injana Formation's sandstones and hypothesized that the clastics came from earlier sedimentary rock and basic igneous and metamorphic rocks. Kettanah and Abdulrahman (2022) investigated the geochemistry and petrography of sandstones of Injana Formation and concluded that the sandstones are immature in terms of composition and textural development ranging between arkose and lithic arkose. Based on major oxide discriminant plots, these sandstones were primarily sourced from intermediate igneous rocks.

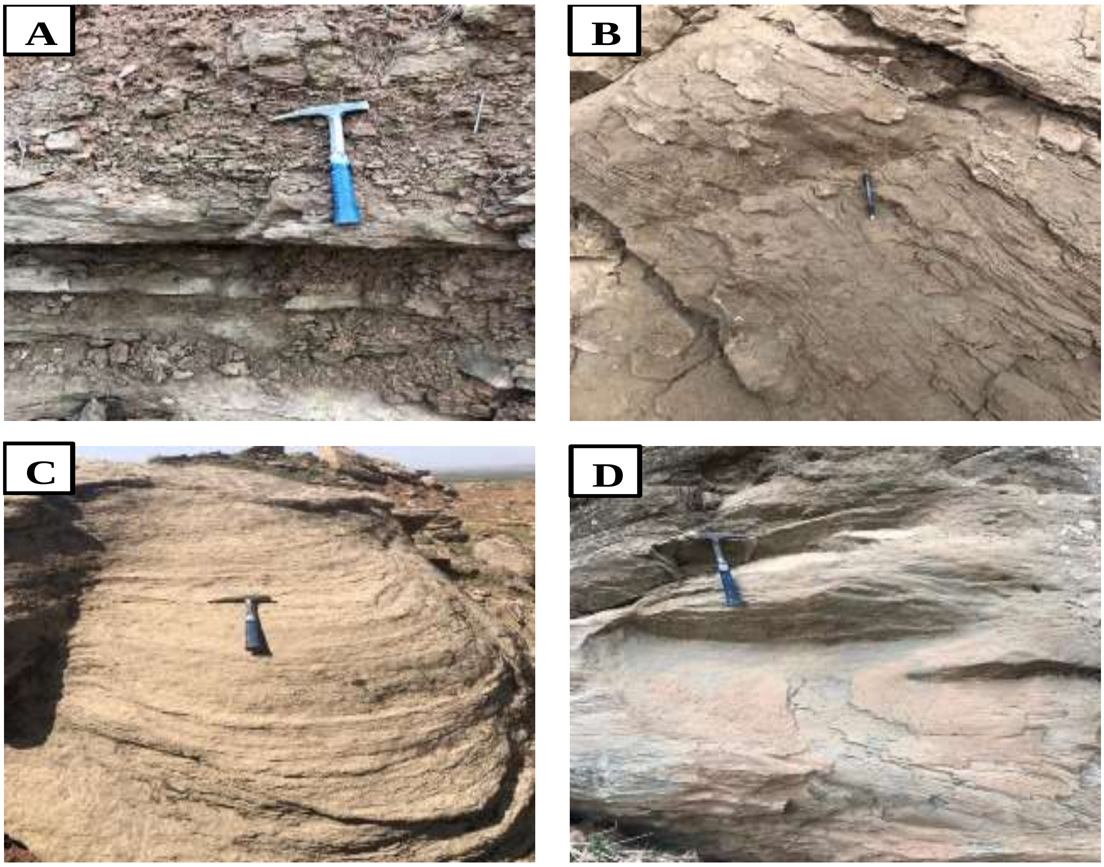

Fig.1. Photographs of the sandstone of Injana Formation (upper Miocene) showing the laminated and cross-laminated sandstone in Degla section (A, B) and Mirawa section (C, D).

The study aims to discuss the major, trace and REE geochemistry for the sandstone of the Injana Formation to infer the provenance, paleoclimate, and paleoweathering of these sandstone rocks through a bulk-rock geochemical data. In broad interest, the results of this study have significant implications to reconstruct paleoclimatic conditions.

Geological setting

During the Late Miocene, most of the shelf units were uplifted as a result of the collision between the Iranian and Anatolian plates with the Arabian plate. A large quantity had been eroded on the elevated area, and the resulting debris was dumped into the nearby molasse basin (Jassim and Goff, 2006). Injana Formation sediments reflect the beginning of molasse sediments created as a result of the collision during the Alpine orogeny (Beydoun, 1993). Injana Formation in Iraq has been observed in the northern and middle regions of the low folded (foothill) zone (LFZ) and some parts of the Mesopotamian foredeep (Fouad, 2012). The type section of the Injana Formation is located at the northeastern border of Jabal Hamrin, where its thickness is 620 m (Jassim *et al.*, 1984). It also extends into Syria (Upper Fars; Ejel and Abdul Rahim, 1974), Turkey (Siirt series; Brinkmann, 1976), and Iran (Upper Fars or Aghajari Formation; James and Wynd, 1965). Injana Formation is composed of fine-grained pre-molasse sediments that were initially deposited in coastal regions and afterward in a fluvial and lacustrine system (Al-Rawi *et al.*, 1992). The Fat'ha and Mukdadiya rocks represent the lower and upper boundaries of Injana Formation respectively (Sissakian, 1992). The investigated Mirawa and Degla sections are situated in the upper folded area of the unstable shelf (Fig. 2).

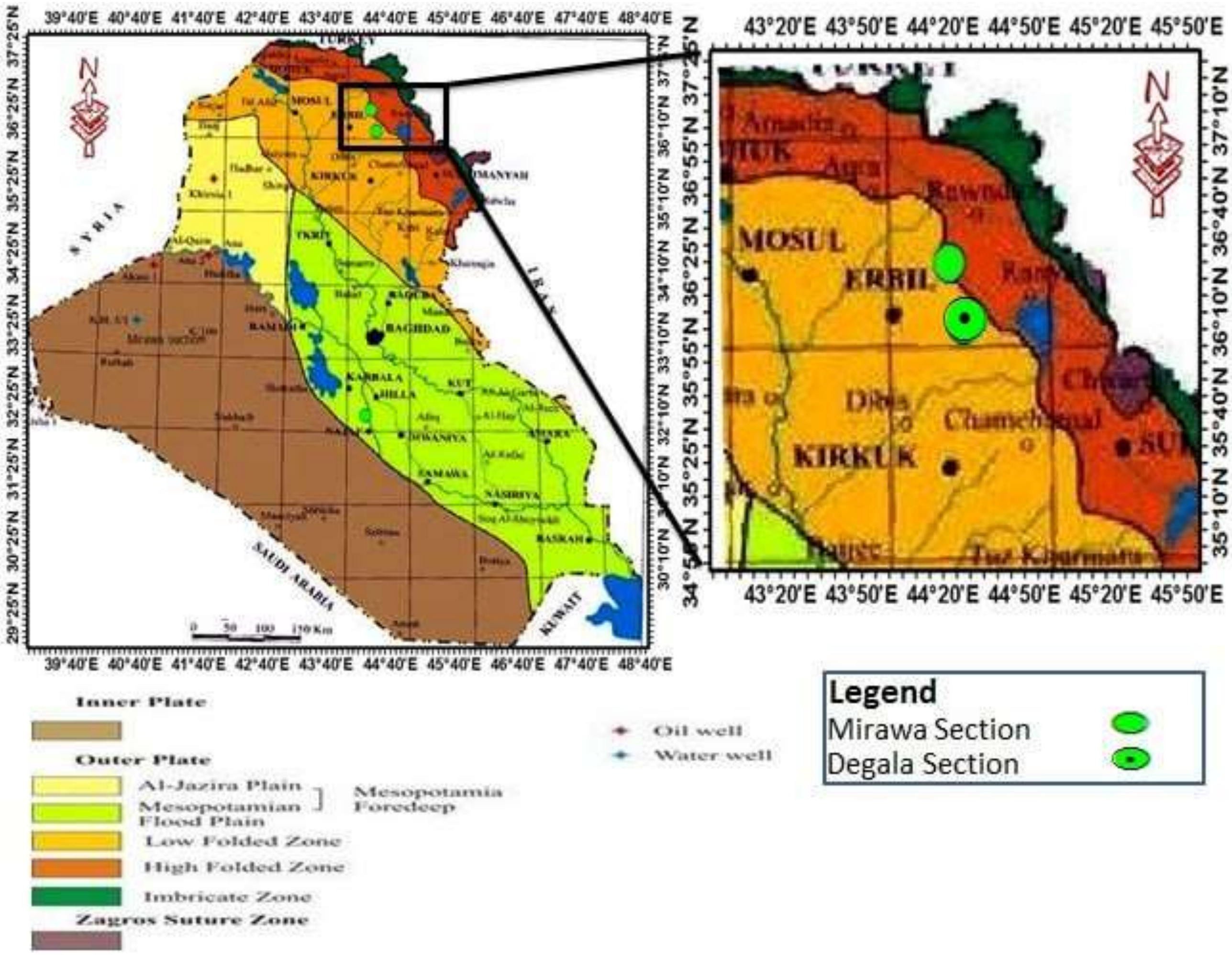

Fig. 2. Tectonic and location map of the studied area (after Fouad, 2015).

Samples and Methods

A geochemical study of sandstone is implemented on 12 sandstone samples distributed in the two sites (6 samples from Degala site "named D ", and 6 samples from Mirawa site "named M "). Major oxides are determined by X-ray fluorescence at Baghdad University (Cu tube target, Ni filter, power: 40 kV, current: 20 mA; speed: 1 cm/min). Trace and rare earth elements are measured using inductively coupled plasma-mass spectrometry (ICP-MS) at Acme Labs in Vancouver, British Columbia, Canada (Code AQ250 EXT REE). The concentrations of the major and trace elements have been compared to the upper continental crust (UCC) and the REEs are normalized to the chondrites and UCC values. For the accuracies of the analysis, sample M17 was analysed three times and the results were highly identical. For the accuracy, an international standared (STD BVGEO01) was used.

Results

Major oxides geochemistry

The content of the major oxides in the analysed sandstone samples are given in Table (1). In all of these samples, SiO_2 is predominated (31.47-40.65%, average 36.84%), Al_2O_3 and CaO contents are in the range of 1.64-9.21% (average 5.14%) and 22.28-30.76% (average 25.3%) respectively. The CaO contents are high in comparison with Fe_2O_3 (1.91-5.25%), MgO (1.69-4.06%), Na_2O (1.02-3.11%), K_2O (0.1-2.58%), and TiO_2 (0.23-0.78%). In contrast, the Injana sandstones have low values of both MnO (0.04-0.26%) and P_2O_5 (0.09-0.63%). The average concentrations of SiO_2, Al_2O_3, Fe_2O_3, Na_2O, K_2O, and TiO_2 of the analyzed samples of Injana Formation are generally lower than the UCC, whereas CaO concentration is much higher than that of the UCC, and MnO, MgO and P_2O_5 are slightly higher than the UCC (Table 1). The ratio of log SiO_2/Al_2O_3 to log Na_2O/K_2O indicates that most of the sandstones under study are primarily plotted in litharenite fields, except for three samples located in graywacke field (Fig. 3).

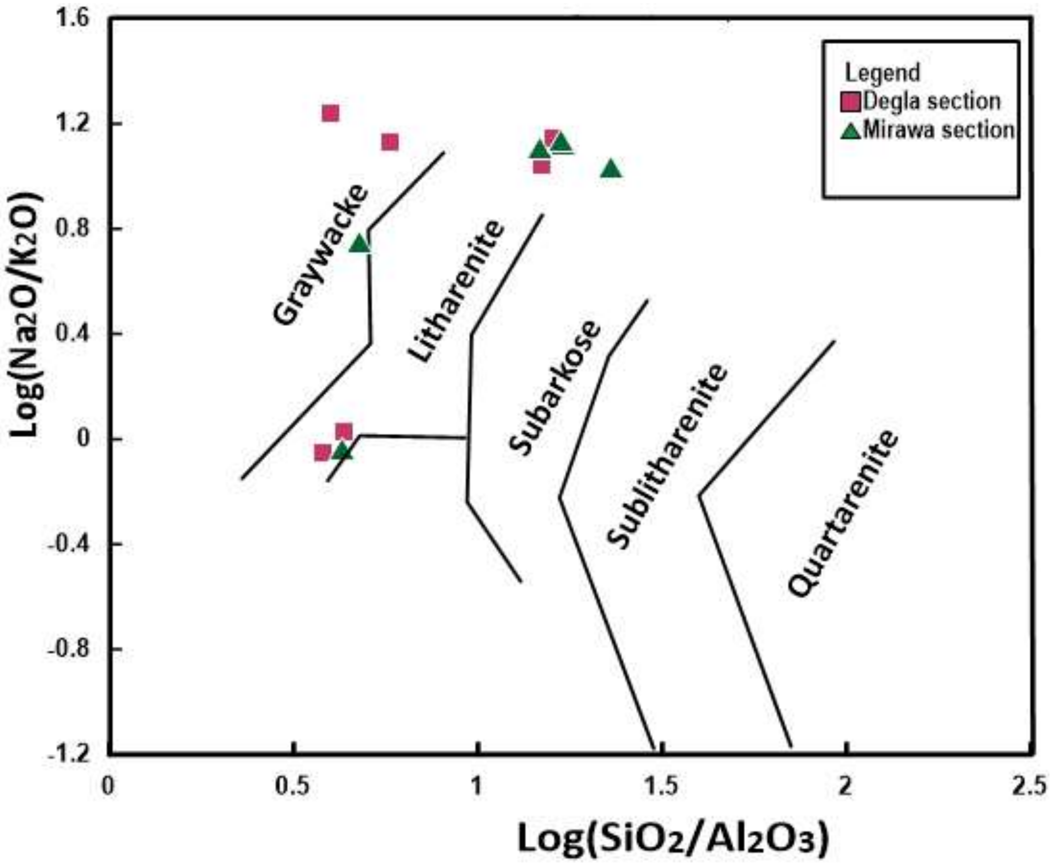

Fig. 3. Log (SiO2/Al2O3) versus log (Na2O/K2O) diagram of the Injana sandstones (Pettijohn *et al.*, 1987).

Table 1: Major oxide contents (in wt.%) and paleoweathering parameters of upper Miocene sandstones from Injana Formation.

Sample No.	SiO_2%	TiO_2%	Al_2O_3%	Fe_2O_3%	MnO%	MgO%	CaO%	Na_2O%	K_2O%	P_2O_5%	LOI%	Total**	CaO*	CIA	CIW	PIA	ICV
Degla section																	
D2	35.98	0.66	8.99	2.83	0.22	3	22.28	2.43	0.14	0.53	22.94	100	0.22	52.46	52.91	52.5	3.49
D6	34.88	0.78	9.21	4.84	0.26	2.29	24.22	1.04	1.18	0.11	21.18	99.99	0.28	66.12	72.83	69.76	3.73
D11	40.65	0.68	2.72	4.23	0.2	2.02	25.59	1.43	0.13	0.59	21.76	100	0.28	35.85	36.52	35.32	12.55
D13	33.26	0.24	7.66	5.25	0.04	4.06	28.29	2.77	2.58	0.09	15.76	100	0.29	39.17	45.7	34.84	5.64
D19	38.25	0.59	6.64	1.91	0.22	2.8	24.69	1.47	0.11	0.54	22.77	99.99	0.28	57.28	57.84	57.42	4.75
D21	40.26	0.73	2.5	4.34	0.21	2.16	22.61	1.66	0.12	0.55	24.88	100.02	0.21	30.89	31.39	30.26	12.67
Mirawa section																	
M1	33.8	0.34	7.08	3.41	0.11	3.39	30.76	3.11	0.55	0.1	17.36	100.01	0.32	39.52	40.87	38.77	5.87
M8	39.53	0.3	2.32	4.03	0.22	3.29	23.1	1.73	0.13	0.57	24.78	100	0.09	28.38	28.86	27.64	14.08
M12	39.8	0.69	2.71	4.99	0.16	1.69	22.5	1.67	0.13	0.61	25.04	99.99	0.18	32.44	33.01	31.81	11.71
M15	37.89	0.76	2.26	3.45	0.21	3.02	22.45	2.2	0.16	0.63	26.97	100	0.2	23.41	23.84	22.42	14.15
M17	31.57	0.77	7.41	3.57	0.18	2.59	27.67	1.02	1.11	0.13	23.97	99.99	0.28	61.85	68.77	64.84	4.96
M22	37.63	0.65	1.64	2.44	0.2	2.56	27.06	1.08	0.1	0.55	26.09	100	0.29	31.07	31.7	30.28	20.64
Min.	31.57	0.24	1.64	1.91	0.04	1.69	22.28	1.02	0.1	0.09	15.76	99.99	0.09	23.41	23.84	22.42	3.49
Max.	40.65	0.78	9.21	5.25	0.26	4.06	30.76	3.11	2.58	0.63	26.97	100.02	0.32	66.12	72.83	69.76	20.64
Average	36.84	0.59	5.14	3.75	0.18	2.76	25.3	1.84	0.65	0.41	22.59	100	0.24	42	44.35	42	9.88
UCC*	55.62	0.64	15.4	5.04	0.1	2.48	3.59	3.27	2.8	0.15				52.74	24.07	16.48	5.87

UCC*: upper continental crust from Rudnick and Gao (2003).
LOI= 100- sum of all major oxides and trace elements
**= Adjuted total

Trace elements geochemistry

Table (2) displays the studied sandstone's trace element concentrations. Commonly, they have a wide range. The Injana Formation sandstone generally has trace element concentrations lower than the UCC averages except Cu (149.92 ppm) and Ni (77.48 ppm) (Fig. 4), where their concentrations are higher. The sandstone has variable Th (1.8-3.20 ppm), U (0.2-0.50 ppm), and Th/U ratio (4.50-15.50) but is consistent with the (UCC). The La/Th, Th/U, Y/Ni, Cr/V, Zr/Sc, Cr/Th, La/Y, Th/Sc, Zr/10, Sc/Cr, and Th*10 ratios are listed in Table (3).

From the UCC-normalized trace element spider diagrams (Fig.4), it seems that the Hf and Zr are severely depleted, Cu is enriched, Ni is slightly enriched; and other elements are slightly depleted.

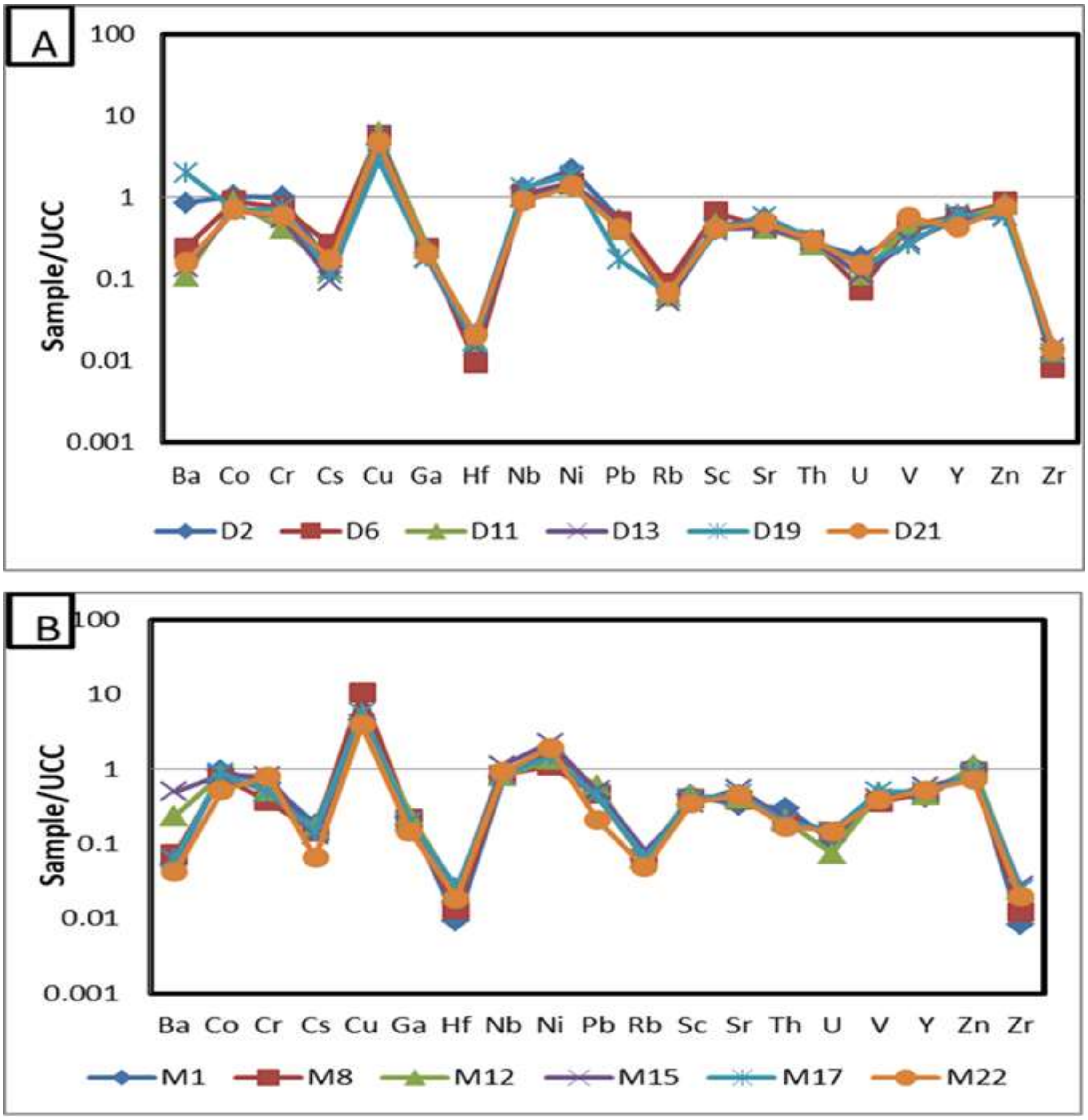

Fig. 4. Spider diagrams showing upper crust-normalized trace element distributions for the late Miocene sandstone from the Injana Formation. (A) Degla section and (B) Mirawa section.

Table 2: Trace element concentrations (in ppm) of Late Miocene sandstone from Injana Formation.

Sample No.	Ba	Co	Cr	Cs	Cu	Ga	Hf	Nb	Ni	Pb	Rb	Sc	Sr	Th	U	V	Y	Zn	Zr
Degla section																			
D2	533.90	17.80	91.80	0.69	123.78	3.60	0.11	15.59	105.10	8.82	6.40	6.10	179.40	2.90	0.50	37.00	12.24	50.20	2.70
D6	148.30	15.40	70.20	1.29	163.44	4.20	0.05	13.14	70.60	8.60	7.40	9.20	136.60	3.10	0.20	45.00	12.18	58.30	1.60
D11	67.50	14.80	38.30	0.66	173.55	4.10	0.09	12.40	66.90	6.79	5.10	6.60	133.90	2.80	0.30	45.00	11.36	54.80	2.50
D13	87.80	12.00	52.00	0.47	161.56	3.10	0.08	12.35	69.10	7.81	4.50	5.80	136.40	3.10	0.30	28.00	11.47	39.30	2.70
D19	1258.20	12.00	67.50	0.58	82.04	3.20	0.09	15.76	87.90	2.89	5.70	5.40	186.10	3.20	0.40	26.00	13.10	38.50	2.30
D21	99.40	12.00	54.20	0.85	134.81	3.60	0.11	10.82	65.10	7.07	5.70	5.80	159.00	3.10	0.40	55.00	9.06	50.70	2.60
Mirawa section																			
M1	33.60	16.30	61.00	0.91	132.33	4.00	0.05	9.50	80.20	8.59	5.40	6.30	105.50	3.20	0.30	41.00	8.89	72.40	1.60
M8	45.40	13.50	34.50	0.72	300.62	3.80	0.07	10.14	52.50	7.95	5.30	5.70	126.40	2.10	0.40	36.00	10.04	62.60	2.40
M12	147.60	14.80	46.30	0.80	139.85	4.30	0.12	9.77	62.90	10.37	5.30	6.30	132.40	2.20	0.20	48.00	9.71	75.50	4.60
M15	313.50	14.40	73.60	0.64	111.24	3.50	0.12	13.66	106.50	8.93	6.70	4.90	175.90	2.30	0.40	40.00	12.51	55.90	5.30
M17	39.20	15.30	45.70	0.73	163.38	3.40	0.14	10.29	70.20	7.69	5.40	5.70	152.30	2.10	0.40	50.00	10.49	60.20	4.80
M22	26.70	8.80	76.10	0.32	112.41	2.60	0.10	11.11	92.70	3.66	4.10	5.00	143.40	1.80	0.40	38.00	11.21	48.40	3.80
Average	233.43	13.93	59.27	0.72	149.92	3.62	0.09	12.04	77.48	7.43	5.58	6.07	147.28	2.66	0.35	40.75	11.02	55.57	3.08
UCC*	624.00	17.30	92.00	4.90	28.00	17.50	5.30	12.00	47.00	17.00	84.00	14.00	320.00	10.50	2.70	97.00	21.00	67.00	193.00

*UCC: upper continental crust from Rudnick and Gao(2003).

Table 3: Elemental ratios of Late Miocene sandstone from Injana Formation.

Sample No.	Th/U	La/Th	Cr/V	Y/Ni	Cr/Th	Zr/Sc	Th/Sc	Y/Ho	La/Y	Sc/Cr	Zr/10	Th*10
Degla section												
D2	5.80	5.14	2.48	0.12	31.66	0.44	0.48	26.61	1.22	0.07	5.02	29.00
D6	15.50	4.26	1.56	0.17	22.65	0.17	0.34	27.68	1.08	0.13	5.83	31.00
D11	9.33	4.71	0.85	0.17	13.68	0.38	0.42	27.05	1.16	0.17	5.48	28.00
D13	10.33	4.55	1.86	0.17	16.77	0.47	0.53	31.86	1.23	0.11	3.93	31.00
D19	8.00	5.34	2.60	0.15	21.09	0.43	0.59	27.29	1.31	0.08	3.85	32.00
D21	7.75	3.68	0.99	0.14	17.48	0.45	0.53	24.49	1.26	0.11	5.07	31.00
Mirawa section												
M1	10.67	3.25	1.49	0.11	19.06	0.25	0.51	26.94	1.17	0.10	7.24	32.00
M8	5.25	5.05	0.96	0.19	16.43	0.42	0.37	31.38	1.06	0.17	6.26	21.00
M12	11.00	4.50	0.96	0.15	21.05	0.73	0.35	30.34	1.02	0.14	7.55	22.00
M15	5.75	6.30	1.84	0.12	32.00	1.08	0.47	29.79	1.16	0.07	5.59	23.00
M17	5.25	5.29	0.91	0.15	21.76	0.84	0.37	30.85	1.06	0.12	6.02	21.00
M22	4.50	6.94	2.00	0.12	42.28	0.76	0.36	32.02	1.12	0.07	4.84	18.00
Average	7.60	4.28	1.45	0.14	22.29	0.51	0.44	28.85	1.03	0.10	5.56	26.58
UCC*	3.89	2.95	0.95	0.45	8.76	13.79	0.75	25.30	1.48	0.15	6.70	105.00

*UCC: upper continental crust from Rudnick and Gao (2003).

Rare earth elements

Table (4) displays the quantities and ratios of the Rare Earth Elements (REE) of the Injana sandstones. The chondrite-normalized REE distribution of the samples (Fig. 5) appears similar to the REE distribution pattern of UCC as reported by Rudnick and Gao (2003). The REE values show enrichment of light REEs (LREEs, La- Eu), as well as a somewhat uniform distribution of heavy REEs (HREEs, Gd-Lu). The quantification of Eu anomaly is calculated as follows: Eu/Eu* ratio $=2*(Eu)_{CN}/(Sm)_{CN} +(Gd)_{CN}$. The ratio of Ce anomaly is calculated using the following equation: $2*(Ce)_{CN} /(La)_{CN} +(Pr)_{CN}$ (Taylor and McLennan, 1985). The subscript ($_{CN}$) refers to chondrite-normalized values (Taylor and McLennan, 1985). The normalized ratios of the REE such as $(La)_N/(Yb)_N$, $(La)_N/(Sm)_N$, $(Gd)_N/(Yb)_N$, $(La)_N/(Nb)_N$: $(Element)_N=(Element)_{Sample} /(Element)_{Chondrite}$ are reported in Table (4).

There is a considerable difference in the total rare earth elements (ΣREE) between 19.02 to 84.13 ppm (average = 54.81 ppm). The ΣREE in sandstone samples is lower than the ΣREE content of the UCC (Average= 63.05) The ΣREE in the sandstones of Injana Formation exhibits relatively positive relationships with Th and P. In contrast, the ΣREE shows no relationships with Al (Fig. 6) implying that these elements may be hosted in accessory minerals. This suggests that phosphate minerals (e.g., apatite, monazite) and opaque minerals may be predominant host minerals for the REEs (Ramos-V´azquez and Armstrong-Altrin, 2019). Lee et al. (1973) found that appetites from the more mafic rocks contained rare earth assemblages richer in the lighter REE. The studied samples have low Zr content (average 3.08 ppm) which is highly lower than that of the UCC (193 ppm). Moreover, the low correlation of REE with Al indicates that REE distribution is not likely to be controlled by the influence of clay minerals. The LREE's content ranges from 16.90 ppm to 75.07 ppm (average= 48.28 ppm), and the HREE's content ranges from 2.12 to 9.06 ppm (average =6.53). The LREE/HREE ratios are from 7.97 to 8.29 ppm (average=7.41). Typically, the Eu/Eu* values exhibit negative anomalies (0.78 to 0.97; average 0.85). The range of the Ce/Ce* anomaly is from 0.82 to 0.98 (average = 0.89). The range of the ratio $(La/Nb)_{CN}$ is 10.50 to 13.05; average = 11.33), whereas the $(Gd/Yb)_{CN}$ and $(La/Sm)_{CN}$ ratios are between 1.62 and 3.36; average = 2.72), and 2.66 and 4.26; average =3.66) respectively.

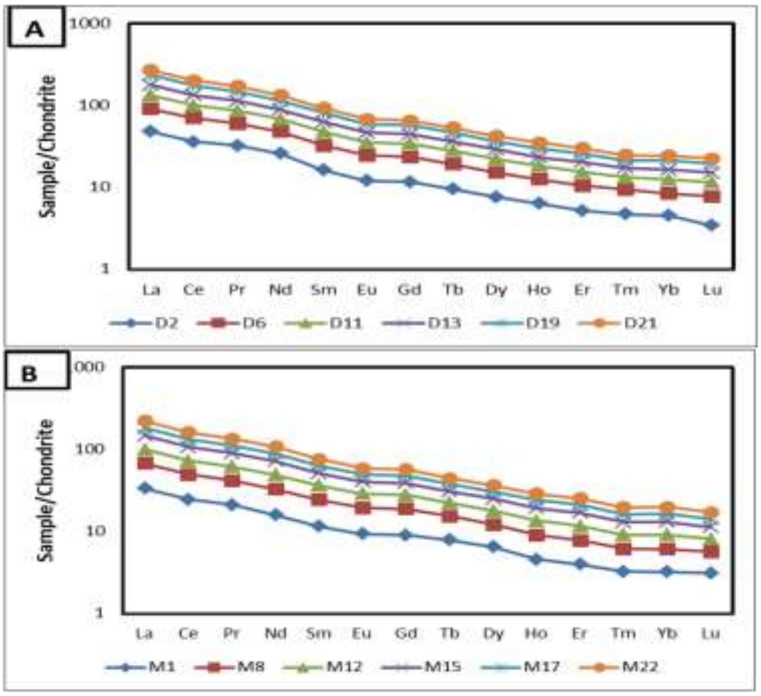

Fig 5. Chondrite- normalized REE patterns for the sandstones of Injana Formation (A) Degala section and (B) Mirawa section.

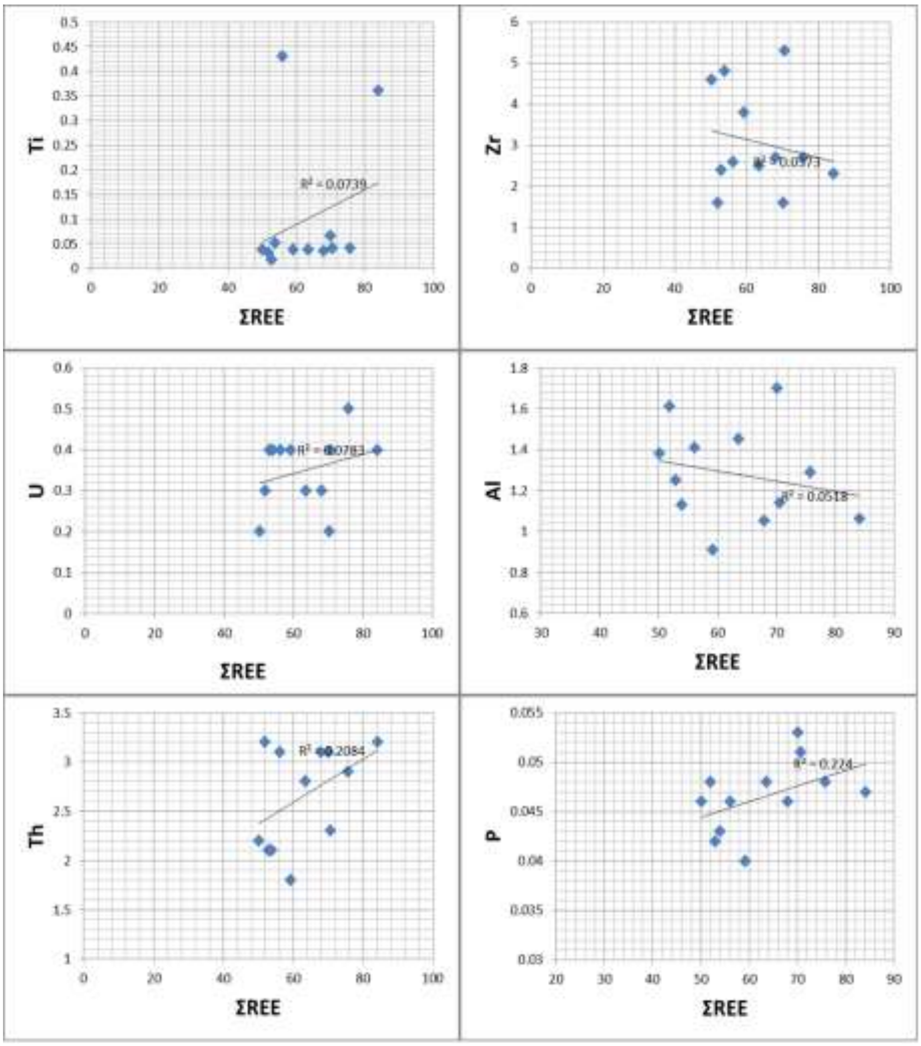

Fig. 6. ΣREE vs. trace elements (Zr, U, Th, Ti, P, and Al) of the study samples of the Injana Formation.

Table 4: Rare earth element Concentrations (ppm) and ratios of rare earth elements of Late Miocene sandstone from the Injana Formation

Sample No.	La	Ce	Pr	Nd	Sm	Eu	Gd	Tb	Dy	Ho	Er	Tm	Yb	Lu	ΣREE	ΣLREE	ΣHREE	ΣLREE /ΣHREE	Eu /Eu*	Ce /Ce*	$(La/Yb)_{CN}$	$(La/Sm)_{CN}$	$(Gd/Yb)_{CN}$
Degla section																							
D2	14.90	28.80	3.87	15.59	3.15	0.80	3.01	0.45	2.46	0.46	1.09	0.16	0.95	0.11	75.80	67.11	8.69	7.72	0.84	0.89	10.62	3.05	2.56
D6	13.20	27.80	3.32	13.14	3.20	0.83	3.10	0.45	2.45	0.44	1.12	0.16	0.81	0.14	70.16	61.49	8.67	7.09	0.85	0.98	11.04	2.66	3.09
D11	13.20	23.10	3.19	12.40	2.93	0.82	2.73	0.42	2.24	0.42	1.01	0.13	0.85	0.12	63.56	55.64	7.92	7.03	0.93	0.82	10.52	2.91	2.59
D13	14.10	26.70	3.26	12.35	3.00	0.73	2.74	0.39	2.24	0.36	1.07	0.14	0.81	0.11	68.00	60.14	7.86	7.65	0.82	0.91	11.79	3.03	2.73
D19	17.10	33.70	4.25	15.76	3.44	0.82	3.28	0.47	2.38	0.48	1.14	0.14	1.03	0.14	84.13	75.07	9.06	8.29	0.79	0.92	11.25	3.21	2.57
D21	11.40	21.90	2.70	10.82	2.33	0.64	2.13	0.34	1.77	0.37	0.90	0.11	0.65	0.10	56.16	49.79	6.37	7.82	0.92	0.91	11.88	3.16	2.65
Mirawa section																							
M1	10.40	19.70	2.54	9.50	2.25	0.69	2.34	0.37	2.08	0.33	0.84	0.11	0.67	0.10	51.92	45.08	6.84	6.59	0.97	0.89	10.52	2.98	2.82
M8	10.60	19.90	2.49	10.14	2.48	0.68	2.54	0.35	1.85	0.32	0.80	0.10	0.61	0.08	52.94	46.29	6.65	6.96	0.88	0.89	11.77	2.76	3.36
M12	9.90	18.70	2.40	9.77	2.35	0.61	2.35	0.33	1.81	0.32	0.82	0.10	0.62	0.08	50.16	43.73	6.43	6.80	0.84	0.89	10.82	2.72	3.06
M15	14.50	27.30	3.42	13.66	2.95	0.70	2.85	0.40	2.30	0.42	1.08	0.13	0.83	0.10	70.64	62.53	8.11	7.71	0.78	0.90	11.83	3.17	2.77
M17	11.10	20.40	2.55	10.29	2.35	0.61	2.32	0.32	1.85	0.34	0.90	0.11	0.71	0.09	53.94	47.30	6.64	7.12	0.84	0.88	10.59	3.05	2.64
M22	12.50	23.10	2.85	11.11	2.39	0.58	2.32	0.33	1.89	0.35	0.89	0.12	0.71	0.10	59.24	52.53	6.71	7.83	0.79	0.89	11.93	3.37	2.64
Average	12.74	24.26	3.07	12.04	2.74	0.71	2.64	0.39	2.11	0.38	0.97	0.13	0.77	0.11	63.05	55.56	7.50	7.41	0.85	0.89	11.20	3.01	2.77
UCC*	31.00	63.00	7.10	27.00	4.70	1.00	4.00	0.70	3.90	0.83	2.30	0.30	2.00	0.31	148.14	133.80	14.34	9.33	0.73	0.98	10.50	4.26	1.62
Chondrite**	0.31	0.808	0.12	0.6	0.19	0.07	0.25	0.04	0.32	0.07	0.21	0.03	0.20	0.03	2.108	2.37	1.19	2					

*UCC: Upper continental Crust from Rudnick and Gao (2003).

** Chondrite:(Taylor and McLennan,1985.)

Discussion

Provenance

The geochemical analysis of the sediments and rocks provides hints to describe the provenance of the clastic sedimentary rocks (Cullers, 2000). Certain trace elements such as Cr, Sc, V. Ni, Co, Y, Nb, Zr, Th, and REEs are frequently used in interpreting the composition and provenance of the source area due to their low propensity for mobility during post-depositional processes (McLennan *et al.,* 1993). Based on diagrams in Figure (7A-C), Th/Co versus La/Sc diagram of Cullers (2000), Co/Th versus La/Sc versus (McLennan *et al.,* 1993), and Cr/Th versus Th/Sc (Totten *et al.,* 2000) show that the Injana Formation samples under study are located close to the field between intermediate and mafic sources. In addition, and from the ternary diagram V-Ni-Th*10 (Bracciali *et al.,* 2007), the Injana sandstones are located around the V-Ni line indicating provenance that is both intermediate and mafic (Fig. 8). The Th/Co, La/Sc Cr/Th, La/Co, and Th/Sc and ratios of the examined Injana sandstones are compared with the UCC (Table 5) to determine the source of these sandstones. According to these ratios, it is found that the mafic rocks are mostly responsible for the composition of these sandstones. Mafic provenance of these sandstones supported by the high concentrations of Cu and Ni; where these two elements are compatible elements and they are associated with ferromagnesian minerals such as olivine and pyroxene. Distribution patterns of the REE, Eu anomalies, and $(Gd/Yb)_{CN}$ ratios in sediments, all provide information about the characteristics of the source region. Mafic source rocks exhibit lower ratios of LREE/HREE, higher ratios of gadolinium (Gd) to ytterbium (Yb) normalized to chondrite (CN), and a lack of europium (Eu) anomalies. In contrast, felsic source rocks display low $(Gd/Yb)_{CN}$ ratios, higher LREE/HREE ratios, and negative Eu anomalies (Cullers, 1994). The Injana sandstone exhibits a comparatively lower ratio of LREE/HREE with an average of 7.41. Additionally, it demonstrates a higher ratio of gadolinium (Gd) to ytterbium (Yb) normalized to chondrite (CN) with an average of 2.77. Furthermore, it displays negative values for europium (Eu) and its corresponding ratio to the average europium value in the UCC (Eu/Eu*) (average = 0.80). The Eu/Eu* ratio is reliable source indicator for Injana sandstones because the plagioclase alteration is low (average PIA= 42%; Table 1) indicating no destroying of the plagioclase of the parent rocks. Destroying the plagioclase leads to removing the Eu that is incorporated in the plagioclase, which will lead to a lower Eu/Eu* value for sediments compared to their source rock (Getaneh and Atnafu, 2020). The Eu/Eu* values of the studied sandstone samples of Injana Formation are in the range of 0.79-0.97. These values are within the mafic rocks range (Table 5).

These observations indicate that the Injana sandstone has been primarily originated from mafic igneous rock sources (Table 4). Yttrium (Y) exhibits chemical characteristics that are analogous to those of Holmium (Ho), thereby leading to its classification within the lanthanides group (Tostevin *et al.,* 2016). According to Song et al. (2014), it has been observed that volcanic ash and terrigenous materials often exhibit Y/Ho values of about 28, but seawater tends to have higher values ranging from 44 to 74. The Y/Ho values recorded in the samples of the current investigation range from 24.48 to 32.02 as shown in Table (3). The aforementioned values are indicative of terrigenous minerals. The La/Co, Th/Co, Th/Sc, Cr/Th, Th/Cr, and La/Sc ratios of the Injana sandstone (0.8 0, 0.94, 0.44, 0.19, 0.04, 22.29 and 2.18, respectively) are compared with those of the UCC (Table 5). This comparison suggests that these sandstones had been originated from intermediate to mafic rocks. This interpretation is consistent with the provenance of the mudrocks of Injana Formation (Al-Maadhidi *et al.,* 2023).

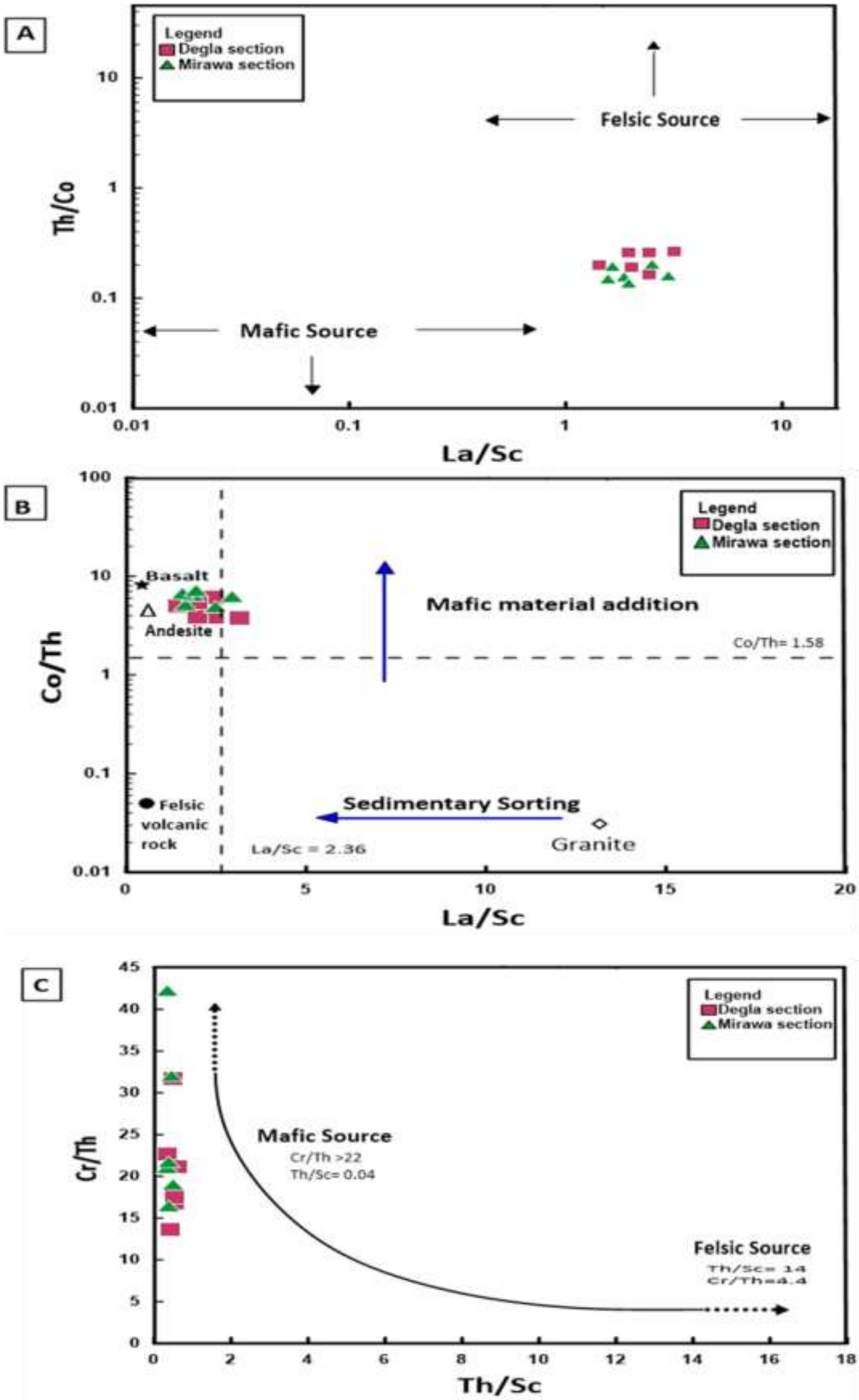

Fig.7. Discrimination diagrams for the Injana sandstones showing the provenance. (A) after Cullers (2000); (B) after McLennan et al. (1993); (C) after Totten et al. (2000).

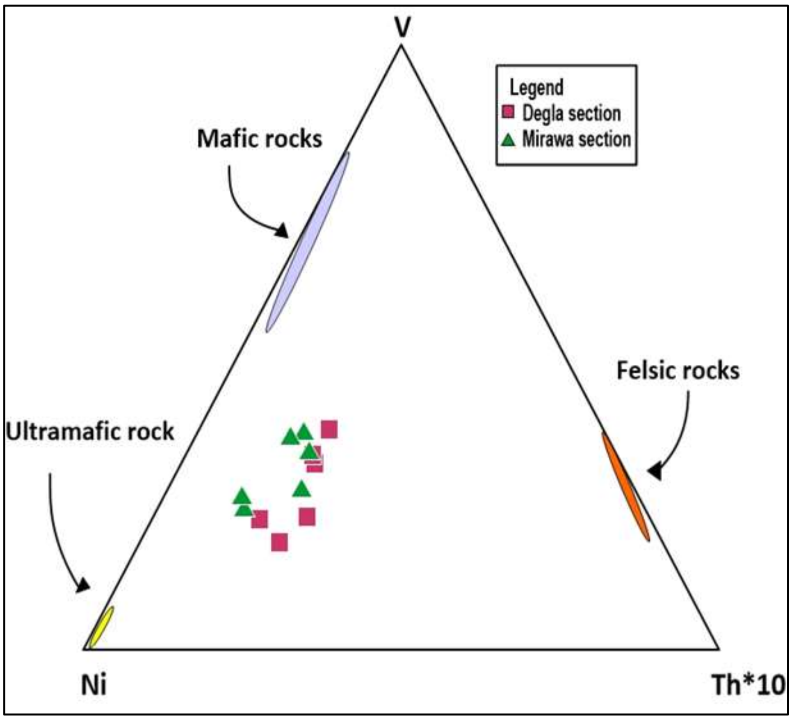

Fig.8. Ternary diagram showing the provenance of the Injana samples (after Bracciali *et al.*, 2007).

Table 5: Elemental ratios of the Injana Sandstone compared with the range values of sediments derived from mafic and felsic rocks, and upper continental crust (Armstrong-Altrin et al., 2013).

Elemental ratio	Studied samples		Range of sediments from mafic sources	Range of sediments from felsic sources	UCC*	PAAS**
	Range	Average				
Eu/Eu*	0.78-0.97	0.80	0.71-0.95	0.40-0.94	0.63	0.71
La/Co	0.63-1.42	0.94	0.38-0.41	1.8-13.8	1.76	0.9
Th/Sc	0.34-0.75	0.44	0.05-0.22	0.84-20.50	0.79	0.9
Th/Co	0.13-0.26	0.19	0.04-1.40	0.67-19.40	0.13	0.63
Th/Cr	0.02-0.07	0.04	0.018-0.046	0.13-2.70	0.3	0.13
Cr/Th	13.68-42.28	22.29	25-100	4.00-15.00	7.76	7.53
La/Sc	1.43-3.16	2.18	0.43-0.86	2.50-16.30	2.21	2.4

*UCC:Upper Continental Cust (Taylor and McLennan,1985)

**PAAS: Post Archean Australian Shale (Taylor and McLennan,1985)

Paleoclimate

The paleoclimate of the source area has been widely interpreted using geochemical proxies (Ge *et al.*, 2019). The graphical plot between SiO_2 and (Al_2O_3+Na_2O + K_2O) can be used to provide palaeoclimatic conditions (Suttner and Dutta, 1986). The examined samples of the Injana Formation have SiO_2 values ranging from 31.57 to 40.65 wt.%, with an average of 36.84 (Table 1). These values suggest an arid paleoclimate. The (Al_2O_3+Na_2O + K_2O) values are between 2.76 to14.9 with an average of 7.63 (Table 1) indicating semi-arid paleoclimate. These data suggest an arid to semi-arid climate during the deposition of the sandstone of the Injana Formation (Fig. 9).

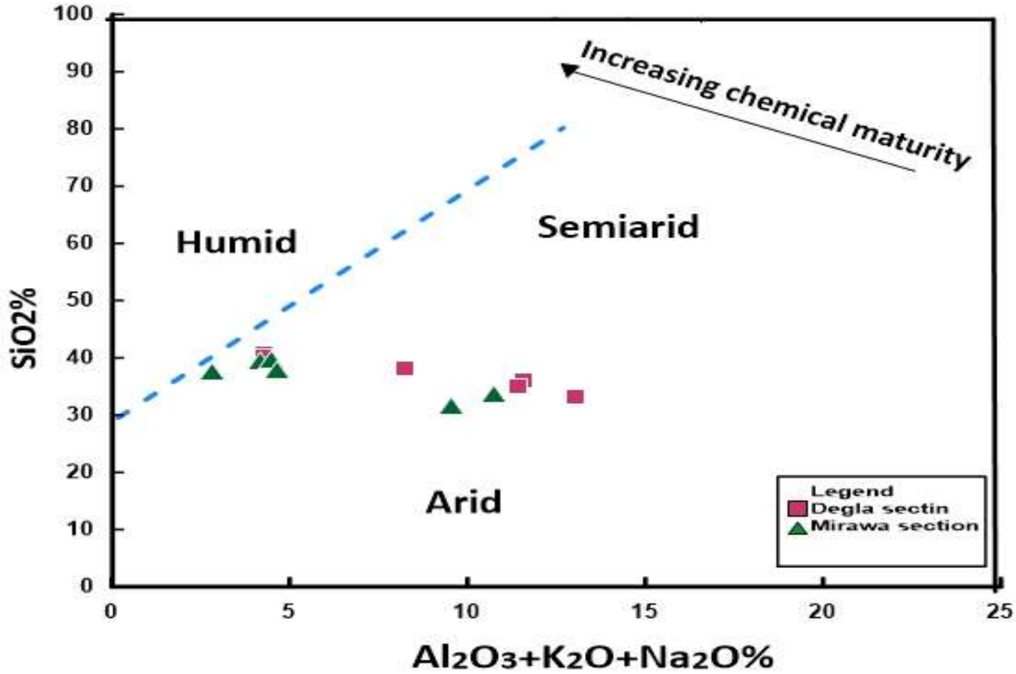

Fig .9. SiO_2 versus (Al_2O_3 + K_2O + Na_2O) to differentiate the climatic conditions during the deposition of the Injana Formation (Suttner and Dutta, 1986).

Source area weathering conditions

Several methods such as the plagioclase index of alteration (PIA) developed by Fedo et al. (1995) can be used to assess the intensity of paleoweathering in the source region. Chemical index of alteration (CIA), the chemical index of weathering (CIW) is suggested by Harnois (1988), while the index of chemical variability (ICV) is developed by Cox et al. (1995), and the A–CN–K diagram is presented by Nesbitt and Young (1982) and Fedo et al. (1995). The mineralogy and geochemistry of clastic deposits and rocks are significantly affected by the presence and extent of chemical weathering (Bokanda *et al.*, 2021). Various indicators of weathering can be employed to evaluate the extent of weathering in sedimentary rocks (e.g., Fedo *et al.*, 1995). These weathering indicators can be used as parameters to understand the climatic conditions during deposition in addition to providing a straightforward statement about the weathering conditions. Low levels of weathering are typically associated with arid or cool and dry climates, whereas high levels of weathering are typically thought to be associated with humid temperate to tropical climates (Chen *et al.*, 2021). The CIA is expressed as CIA = [(Al_2O_3)/ (K_2O+ Al_2O_3+ + Na_2O+ CaO*)] × 100, where CaO, Al_2O_3, K_2O, and Na_2O are in molar proportion and CaO* is the CaO restricted to calcium derived from silicate minerals (Nesbitt and Young, 1982). Since the studied sandstone is rich in carbonate cement, the method employed in this investigation to acquire CaO* is based on that proposed by McLennan et al. (1993). CaO*= CaO-(3.33*P_2O_5). If the corrected molar CaO value exceeds the Na_2O value, the CaO* value is considered valid as the Na_2O value. Conversely, if the CaO* value is equal to or less than the Na_2O value, it is presumed to represent the CaO content.

According to Taylor and McLennan (1985), the Injana sandstone's CIA values (23.41-66.12, average 42) are more asymptotic than those of the UCC indicating that its parent rocks underwent low to moderate weathering. The chemical weathering level can be determined using the CIA vs. (Al_2O_3/Na_2O) plot (Selvaraj and Chen 2006). According to this plot, all the analyzed samples of Injana Formation are located in the low to moderate weathering field (Fig. 10).

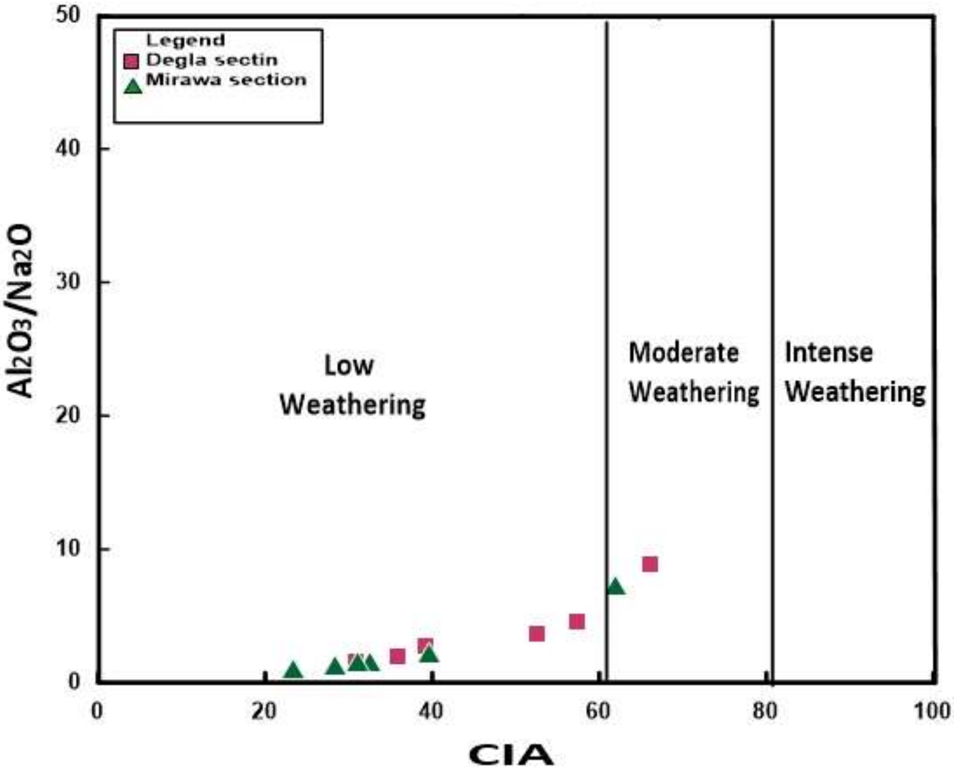

Fig. 10. Scatter plots of CIA versus (Al_2O_3/Na_2O) of the Injana samples (after Selvaraj and Chen, 2006).

The chemical weathering degree and the variations in the primary components and mineralogy during the weathering processes are shown in a ternary plot of A-CN-K (Fig. 11). All of the Injana Formation samples that have been plotted on this diagram are grouped parallel to the A-CN junction between the K-feldspar -plagioclase-–line (Fig. 10). This indicates that the source area of these sandstone samples of Injana Formation is affected by low to medium levels of chemical weathering (McLennan *et al.*, 1993). The depressed CIA values may reflect the lower proportion of feldspars than clay minerals in the examined samples (Tobia and Shangola, 2016). Thus, the diagenetic alteration of feldspar and short-distance transport were the most important factors in augmenting feldspar in sandstone.

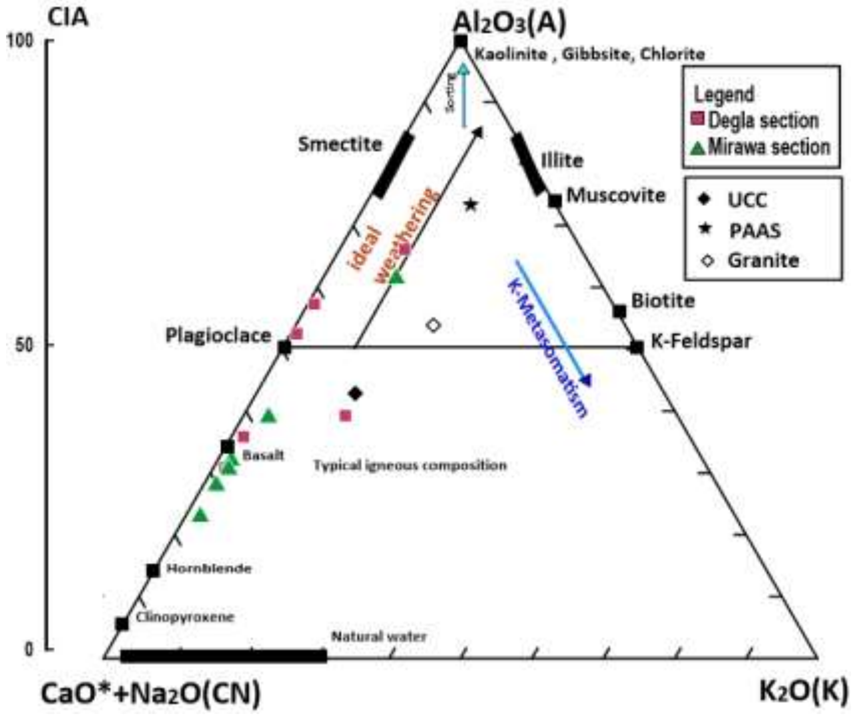

Fig. 11. The A–CN–K diagram of sandstone samples from Injana Formation (after Xu *et al.*, 2011).

The conclusion additionally indicates a single low to moderate weathering rate rather than multiple sedimentary cycles due to the low ICV values of Injana sandstone. Also, the CIW (CIW= [(Al_2O_3)/ (Al_2O_3+ Na_2O+CaO*)] ×100 values range between 23.84 and72.83 with an average = 44.35 (Table 1). These CIW readings reveal the source rocks or sediments with low to moderate stages of chemical weathering (Harnois, 1988)). The PIA (PIA = [(Al_2O_3-K_2O)/ (Al_2O_3+CaO*+ Na_2O - K_2O)] × 100) values range between 22.42 and 69.76 with an average = 42 (Table 1) suggesting low plagioclase weathering of the parent rocks (Fedo *et al.,* 1995).

Paleoweathering assessment also employed the indicator of chemical variability (ICV) (Cox et al. 1995). ICV= (CaO+Na_2O+K_2O+Fe_2O_3+TiO_2+MgO)/Al_2O_3). According to Harnois (1988), immature sediments are indicated by an ICV value higher than 1, and mature sediments are indicated by an ICV value less than 1. This formula shows that alteration products like muscovite, kaolinite, and illite have ICV values are less than 1 (<1), while rock forming minerals such as olivine, pyroxenes, feldspars, and amphiboles have ICV values more than 1 (>1) (Cullers and Podkovyrov, 2000). The Injana sandstone's ICV values range from 3.49 to 20.64 with an average of 9.88 (Table 1) indicating that they are linked to alteration products such as feldspars, amphiboles, and pyroxenes. So, according to Ivanova et al. (2018), the ICV values of the examined sandstones indicate evidence of poor weathering in the source location conditions. ICV values >1 is typically present in the studied samples of the Injana Formation indicating a high impact of short-distance transportation and low weathering of sediment under arid to semi-arid conditions. The results of the paleoweathering conditions are similar to the results of the Kettanah et al. (2022) study of the Injana Formation in the Hemrin South Mountain area.

Scandium and thorium are not separated chemically during the sedimentary process because they are chemically stable (Hou *et al.,* 2018). The enrichment of zircon during the sedimentary cycle causes the ratio of Zr/Sc to rise, whilst the ratio of Th/Sc practically remains the same (Roddaz *et al.,* 2005; Qadrouh *et al.,* 2021). Consequently, sedimentary recycling can be assessed using the plot of Zr/Sc versus Th/Sc. Injana samples' Zr/Sc ratios are precisely proportional to their Th/Sc ratios as seen in Figure (12) far away from the trend line of compositional variations.

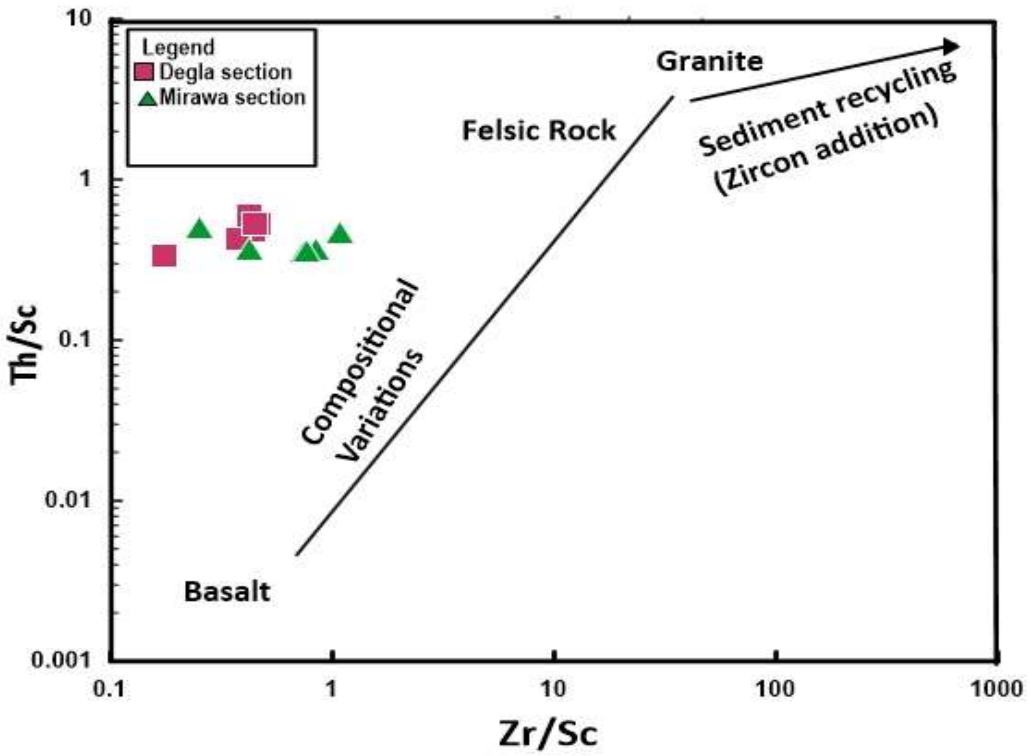

Fig. 12. Th/Sc versus Zr/Sc plot of the Injana sandstone samples after McLennan et al. (1993).

Conclusions

The elemental ratios of the major, trace and REEs of the examined sandstone samples of Injana Formation from northern Iraq show that these samples are derived from intermediate-mafic source rocks. These samples have a low ratio of LREE/HREE, as well as a greater $(Gd/Yb)_{CN}$ ratio. These sandstones also display negative Eu/Eu* anomalies, which are indicative of the influence of mafic igneous processes. These ratios also suggest that the source area had a predominance of low to moderate chemical weathering processes, mostly occurring within an arid to semi-arid climate.

References

Al-Juboury, A.I., McCann, T. and Ghazal, M.M., 2009. Provenance of Miocene Sandstones in Northern Iraq: Constraints from Framework Petrography, Bulk-Rock Geochemistry and Mineral Chemistry, Russian Geology and Geophysics, vol. 50, pp. 517-534. https://doi.org/10.1016/j.rgg.2008.09.005

Al-Juboury, A.I., 1994. Petrology and Provenance of the Upper Fars Formation (Upper Miocene), Northern Iraq. Acta Geologica Univ. Comen. Bratislava, 50, pp. 45-53.

Al-Juboury, A.I.A., 2009. The upper Miocene Injana (upper Fars) Formation of Iraq: Insights on Provenance History. Arabian Journal of Geosciences, 2, pp. 337-364.

Al-Maadhidi, A.S., Kadhim, L.S. and Alkhafaji, M.W., 2023. Trace and Rare Earth Elements Geochemistry of the Mudstone Rocks from the Injana Formation: Implications for Provenance and Paleoclimate. The Iraqi Geological Journal, pp. 159-174. https://doi.org/10.46717/igj.56.2B.12ms-2023-8-21

Al-Rawi, Y.T., Sayyab, A.S., Al-Jassim, J.A., Tamar-Agha M., Al-Sammarai, A.H.I., Karim, S.A., Basi, M.A., Hagopian, D., Hassan, K.M., Al-Mubarak, M., Al-Badri, A., Dhiab, S.H., Faris, F.M. and Anwar, F., 1992. New Names for Some of the Middle Miocene-Pliocene Formations of Iraq. (Fat`ha, Injana, Mukdadiya and Bai Hassan Formations). Iraqi Geol. Jour., Vol.25, no.1, (issued 1993). pp.1-7.

Al-Salmani, N.Z. and Tamar-Agha, M.Y., 2018. Petrography and Provenance of the Sandstone of Injana and Mukdadiya Formations (Upper Miocene/Pliocene) at Duhok Governorate, Northern Iraq. Iraqi Journal of Science, pp .2040-2052.

Al-Sammarai, K.I., 1978. Petrology of the Upper Fars Sandstones and the Origin of Their Cement. Unpublished M.Sc. thesis, University of Baghdad, 141 P.

Armstrong-Altrin, J.S., Nagarajan, R., Madhavaraju, J., Rosalez-Hoz, L., Lee, Y.I., Balaram, V., Cruz-Martínez, A., Avila-Ramírez, G., 2013. Geochemistry of the Jurassic and Upper Cretaceous Shales from the Molango Region, Hidalgo, Eastern Mexico: Implications of Source Area Weathering, Provenance, and Tectonic Setting. Comptes Rendus Geoscience 345, pp. 185-202. https://doi.org/10.1016/j.crte.2013.03.004

Beydoun, Z.R., 1993. Evolution of the Northeastern Arabian Plate Margin and Shelf. Hydrocarbon Habitat and Conceptual Future Potential. Revue de 1. Institute Francais du Petrole, Vol.48, pp. 311-345. https://doi.org/10.2516/OGST%3A1993021

Bokanda, E.E., Fralick, P., Ekomane, E., Bisse, S.B., Tata, C.N., Ashukem, E.N., Belinga, B. C., 2021. Geochemical Constraints on the Provenance, Paleoweathering and Maturity of the Mamfe Black Shales, West Africa. J. Afr. Earth Sci. 175, 104078. https://doi.org/10.1016/j.jafrearsci.2020.104078

Bracciali, L., Marroni, M., Pandolfi, L., Rocchi, S., 2007. Geochemistry and Petrography of Western Tethys Cretaceous Sedimentary Covers (Corsica and Northern Apennines): from Source Areas to Configuration of Margins. In: Arribas, J., Critelli, S., Johnsson, M.J. (Eds.), Sedimentary Provenance and Petrogenesis: Perspectives from Petrography and Geochemistry. Geological Society of America, Special Paper. 420, pp. 73–93. https://doi.org/10.1130/2006.2420(06)

Brinkmann, R., 1976. Geology of Turkey. New York: Elsevier.

Chen, G., Robertson, A.H.F., 2020. User's Guide to the Interpretation of Sandstones Using Whole-Rock Chemical Data, Exemplified by Sandstones from Triassic to Miocene Passive and Active Margin Settings from the Southern Neotethys in Cyprus. Sedimentary Geology 400, 105616. https://doi.org/10.1016/j.sedgeo.2020.105616

Chen, Q., Li, Z., Dong, S., Yu, Q., Zhang, C., Yu, X., 2021b. Applicability of Chemical Weathering Indices of Eolian Sands from the Deserts in Northern China. CATENA 198, 105032. https://doi.org/10.1016/j.catena.2020.105032

Cox R., Lowe D.R., Cullers R.L., 1995. The Influence of Sediment Recycling and Basement Composition on the Evolution of Mudrock Chemistry in the Southwestern United States. Geochimica et Cosmochimica Acta 59(14), pp. 2919-2940. https://doi.org/10.1016/0016-7037(95)00185-9

Cullers R.L., Podkovyrov V.N.., 2000. Geochemistry of the Mesoproterozoic Lakhanda Shales in southeastern Yakutia, Russia: Implications for Mineralogical and Provenance Control, and Recycling. Precambrian Res 104, pp. 77–93. https://doi.org/10.1016/S0301-9268(00)00090-5

Cullers, R.L., 1994. The Controls on the Major and Trace Element Variation of Shales, Siltstones, and Sandstones of Pennsylvanian-Permian Age from Uplifted Continental Blocks in Colorado to Platform Sediment in Kansas, USA. Geochimica et Cosmochimica Acta, 58(22), pp. 4955-4972. https://doi.org/10.1016/0016-7037(94)90224-0

Cullers, R.L., 2000. The Geochemistry of Shales, Siltstones and Sandstones of Pennsylvanian-Permian Age, Colorado, USA: Implications for Provenance and Metamorphic Studies. Lithos 51, pp. 181–203. https://doi.org/10.1016/S0024-4937(99)00063-8

Ejel, F., Abdul Rahim, A.H., 1974. Geology of Syria. Damascus: Dar AlFikr; (In Arabic)

Fedo, C.M., Nesbitt H.W., Young G.M., 1995. Unravelling the Effects of Potassium Metasomatism in Sedimentary Rocks and Paleosols, with Implications for Paleoweathering Conditions and Provenance. Geology 23(10), pp. 921–924. https://doi.org/10.1130/0091-7613(1995)023%3C0921:UTEOPM%3E2.3.CO;2

Floyd, P.A., Leveridge, B.E., 1987. The Tectonic Environment of the Devonian Gramscatho Basin, South Cornwall: Framework Mode and Geochemical Evidence from Turbiditic Sandstones. Journal of the Geological Society of London 144, pp. 531–542. https://doi.org/10.1144/gsjgs.144.4.0531

Fouad, S.F. A., 2015. Tectonic Map of Iraq, Scale 1: 1000 000, 3rd Edition, 2012', Iraqi Bulletin of Geology and Mining, 11(1), p. 8. https://doi.org/10.2118/92339-MS

Fouad, S.F., 2012. Tectonic Map of Iraq, Scale 1: 1000 000, 3rd Edition. Iraq Geological Survey Publications, Baghdad, Iraq.

Garzanti, E., 2019. Petrographic Classification of Sand and Sandstone. Earth-Science Reviews 192, pp. 545–563. https://doi.org/10.1016/j.earscirev.2018.12.014

Garzanti, E., Andò, S., Vezzoli, G., 2008. Settling Equivalence of Detrital Minerals and Grainsize Dependence of Sediment Composition. Earth and Planetary Science Letters 273, pp. 138–151. https://doi.org/10.1016/j.epsl.2008.06.020

Ge, X., Mou, C., Yu, Q., Liu, W., Men, X., He, J., 2019. The Geochemistry of the Sedimentary Rocks from the Huadi No. 1 Well in the Wufeng-Longmaxi Formations (Upper Ordovician-Lower Silurian), South China, with Implications for Paleoweathering, Provenance, Tectonic Setting and Paleoclimate. Marine and Petroleum Geology 103, pp. 646–660. https://doi.org/10.1016/j.marpetgeo.2018.12.040

Getaneh, W. and Atnafu, B., 2020. Geochemistry and Lithostratigraphy of the Mugher Mudstone: Insights into the Late Jurassic-Early Cretaceous Clastic Sedimentation in Ethiopia and its Surroundings. Journal of African Earth Sciences, 164, p.103770. https://doi.org/10.1016/j.jafrearsci.2020.103770

Harnois, L., 1988. The CIW index: a New Chemical Index of Weathering. Sedimentary Geology 55, pp. 319–322. https://doi.org/10.1016/0037-0738(88)90137-6

Hou, Q., Mou, C.L., Wang, Q.Y., Tan, Z.Y., Ge, X.Y., 2018. Geochemistry of Sandstones from the Silurian Hanxia Formation, North Qilian Belt, China: Implication for Provenance, Weathering and Tectonic Setting. Geochem. Int. 56, pp. 362–377. https://doi.org/10.3389/feart.2024.1334982

Ivančič, K., Trajanova, M., Skaberne, D., Šmuc, A., 2018. Provenance of the Miocene Slovenj Gradec Basin Sedimentary Fill, Western Central Paratethys. Sedimentary Geology 375, pp. 256–267. https://doi.org/10.1016/j.sedgeo.2017.11.002

James, G.A. and Wynd, J.G., 1965. Stratigraphic Nomenclature of Iranian Oil Consortium Agreement Area. AAPG bulletin, 49(12), pp. 2182-2245. https://doi.org/10.1306/A663388A-16C0-11D7-8645000102C1865D

Jassim, S.Z., Karim, S., Basi, M.A., Al-Mubarak, M., Munir, J., 1984. Final Report on the Regional Geological Survey of Iraq, Vol. 3, stratigraphy, St. Origin, Min., D.G. Geol. Survev., Min., Inv., 498 P.

Jassim, S.Z. and Goff, J.C., 2006. Geology of Iraq. Dolin, Prague and Moravian Museum, Brno. 341 P.

Kettanah, Y.A. and Abdulrahman, A.S., 2022. Petrography and Geochemistry of Sandstones from the Injana Formation, Hemrin South Mountain, Northern Iraq: Implications for Provenance, Weathering and Tectonic Setting. Geological Journal, 57(5), pp. 2007-2023. https://doi.org/10.1002/gj.4394

Lee, T.D., 1973. A Theory of Spontaneous T Violation. Physical Review D, 8(4), p.1226. https://doi.org/10.1103/PhysRevD.8.1226

Long, X., Yuan, C., Sun, M., Xiao, W., Wang, Y., Cai, K., Jiang, Y., 2012. Geochemistry and Nd Isotopic Composition of the Early Paleozoic Flysch Sequence in the Chinese Altai, Central Asia: Evidence for a Northward-Derived Mafic Source and Insight into Nd Model Ages in Accretionary Orogen. Gondwana Res. 22, pp. 554–566. https://doi.org/10.1016/j.gr.2011.04.009

Löwen, K., Meinhold, G., Güngör, T., 2018. Provenance and Tectonic Setting of Carboniferous–Triassic Sandstones from the Karaburun Peninsula, Western Turkey: A Multimethod Approach with Implications for the Palaeotethys Evolution. Sedimentary Geology 375, pp. 232–255. https://doi.org/10.1016/j.sedgeo.2017.11.006

Mahdi, H.Kh.M., 2006. Sedimentological Study of Injana Formation in Baqaq, Bashiqa and Mandan Areas, Northern Iraq. M.Sc. Thesis, University of Mosul, Iraq (in Arabic, unpublished), 129 P.

McLennan, S.M., Hemming, S., McDaniel, D.K., Hanson, G.N., 1993. Geochemical Approaches to Sedimentation, Provenance, and Tectonics. In: Johnsson, M.J., Basu, A. (Eds.), Processes Controlling the Composition of Clastic Sediments: Boulder, Colorado. Geological Society of America, Special Paper vol. 284, pp. 21–40.

McLennan, S.M., Taylor, S.R. and Kröner, A., 1983. Geochemical evolution of Archean Shales from South Africa. I. The Swaziland and Pongola Supergroups. Precambrian Research, 22(1-2), pp.93-124. https://doi.org/10.1016/0301-9268(83)90060-8

McLennan, S.M., Taylor, S.R., 1991. Sedimentary Rocks and Crustal Evolution: Tectonic Setting and Secular Trends. The Journal of Geology 99, pp. 1–21. http://dx.doi.org/10.1086/629470

Moghaddam, S.P., Salehi, M.A., Jafarzadeh, M., Zohdi, A., 2020. Provenance, Palaeoweathering and Tectonic Setting of the Ediacaran Bayandor Formation in NW Iran: Implications for the Northern Gondwana Continental Margin During the Late Neoproterozoic. Journal of African Earth Sciences 161, 103670. https://doi.org/10.1016/j.jafrearsci.2019.103670

Nesbitt, H.W., Young, G.M., 1982. Early Proterozoic Climates and Plate Motions Inferred from Major Element Chemistry of Lutites. Nature 299, pp. 715–717. https://doi.org/10.1038/299715a0

Nesbitt, H.W., Young, G.M., McLennan, S.M., Keays, R.R., 1996. Effects of Chemical Weathering and Sorting on the Petrogenesis of Siliciclastic Sediments, with Implications for Provenance Studies. The Journal of Geology 104, pp. 525–542. http://dx.doi.org/10.1086/629850

Pettijohn, F.J., Potter, P.E., Siever, R., Pettijohn, F.J., Potter, P.E. and Siever, R., 1987. Introduction and Source Materials. Sand and Sandstone, pp. 1-21.

Qadrouh, A.N., Alajmi, M.S., Alotaibi, A.M., Baioumy, H., Almalki, M.A., Alyousif, M.M., Salim, A.M.A., Rogaib, A.M.B., 2021. Mineralogical and Geochemical Imprints to Determine the Provenance, Depositional Environment, and Tectonic Setting of the Early Silurian Source Rock of the Qusaiba Shale, Saudi Arabia. Mar. Petrol. Geol. 130 ,105131. https://doi.org/10.1016/j.marpetgeo.2021.105131

Ramos-Vázquez, M.A. and Armstrong-Altrin, J.S., 2019. Sediment Chemistry and Detrital Zircon Record in the Bosque and Paseo del Mar Coastal Areas from the Southwestern Gulf of Mexico. Marine and Petroleum Geology, 110, pp. 650-675. https://doi.org/10.1016/j.marpetgeo.2019.07.032

Roddaz, M., Said, A., Guillot, S., Antoine, P.-O., Montel, J.-M., Martin, F., Darrozes, J., 2011. Provenance of Cenozoic Sedimentary Rocks from the Sulaiman Fold and Thrust Belt, Pakistan: Implications for the Palaeogeography of the Indus Drainage System. Journal of the Geological Society 168, pp. 499–516. https://doi.org/10.1144/0016-76492010-100

Roddaz, M., Viers, J., Brusset, S., Baby, P., H´erail, G., 2005. Sediment Provenances and Drainage Evolution of the Neogene Amazonian Foreland Basin. Earth Planet Sci. Lett. 239, pp. 57–78. https://doi.org/10.1016/j.epsl.2005.08.007

Roy, P.D., Caballero, M., Lozano, R., Smykatz-Kloss, W., 2008. Geochemistry of Late Quaternary Sediments from Tecocomulco Lake, Central Mexico: Implication to Chemical Weathering and Provenance. Chemie der Erde-Geochemistry 68, pp. 383–393. https://doi.org/10.1016/j.chemer.2008.04.001

Rudnick, R.L., Gao, S., 2003. Composition of the Continental Crust. In: Holland, H.D., Turekian, K.K. (Eds.), Treatise on Geochemistry. Vol. 3. Elsevier-Pergamon, Oxford, pp. 1–64. https://doi.org/10.1016/j.chemer.2009.05.005

Selvaraj K, Chen CTA., 2006 Moderate Chemical Weathering of Subtropical Taiwan: Constraints from Solid-Phase Geochemistry of Sediments and Sedimentary Rocks. J Geol 114, pp. 101–116.

Sissakian, V.K., 1992. The Geology of Kirkuk Quadrangle, Sheet Ni-38-2, Scale 1: 250000. http://Dx.Doi.Org/10.13140/Rg.2.1.5109.0642

Song, E., Nelson, B.L. and Pegden, C.D., 2014. Advanced Tutorial: Input Uncertainty Quantification. In Proceedings of the Winter Simulation Conference 2014, pp. 162-176. IEEE. https://doi.org/10.1109/WSC.2014.7019886

Suttner, L.J., Dutta, P.K., 1986. Alluvial Sandstone Composition and Paleoclimate I. Framework Mineralogy. Journal of Sedimentary Research 56, pp. 329–345. https://doi.org/10.1306/212F8909-2B24-11D7-8648000102C1865D

Taylor, S.R., McLennan, S.M., 1985. The Continental Crust: Its Composition and Evolution. Blackwell, Oxford, 312 P. https://doi.org/10.1017/S0016756800032167

Tobia F.H, Shangola S. S., 2016. Mineralogy, Geochemistry, and Depositional Environment of the Beduh Shale (lower Triassic), Northern Thrust Zone, Iraq. Turkish Journal of Earth Sciences, 25(4), pp. 367-391. https://doi.org/10.3906/yer-1511-10

Tostevin, R., Shields, G.A., Tarbuck, G.M., He, T., Clarkson, M.O. and Wood, R.A., 2016. Effective Use of Cerium Anomalies as a Redox Proxy in Carbonate-Dominated Marine Settings. Chemical Geology, 438, pp. 146-162. https://doi.org/10.1016/j.chemgeo.2016.06.027

Totten, M.W., Hanan, M.A., Weaver, B.L., 2000. Beyond Whole-Rock Geochemistry of Shales: the Importance of Assessing Mineralogical Controls for Revealing Tectonic Discriminants of Multiple Sediment Sources for the Ouachita Mountain Flysch Deposits. Geological Society of America Bulletin 112, pp. 1012–1022. https://doi.org/10.1130/0016-7606(2000)112%3C1012:BWGOST%3E2.0.CO;2

Xu, Z., Lu, H., Zhao, C., Wang, X., Su, Z., Wang, Z., Liu, H., Wang, L., Lu, Q., 2011. Composition, Origin and Weathering Process of Surface Sediment in Kumtagh Desert, Northwest China. J. Geogr. Sci. 21, pp. 1062–1076. http://dx.doi.org/10.1007%2Fs11442-011-0900-3

Yan, Z., Xiao, W., Wang, Z., Li, J., 2007. Integrated Analyses Constraining the Provenance of Sandstones, Mudstones, and Conglomerates, a Case Study: the Laojunshan Conglomerate, Qilian orogen, Northwest China. Canadian Journal of Earth Sciences 44, pp. 961–986. https://doi.org/10.1139/e07-010

Zaid, S.M., Elbadry, O., Ramadan, F., Mohamed, M., 2015. Petrography and Geochemistry of Pharaonic Sandstone Monuments in Tall San Al Hagr, Al Sharqiya Governorate, Egypt: Implications for Provenance and Tectonic Setting. Turkish Journal of Earth Sciences 24, pp. 344–364. https://doi.org/10.3906/yer-1407-20